PRELIMINARY CONCEPT OF A SPACE-BASED RADAR FOR DETECTING MM-SIZE SPACE DEBRIS

D. Cerutti-Maori[(1)], J. Rosebrock[(1)], I. O. Maouloud[(1)], L. Leushacke[(1)], and H. Krag[(2)]

[(1)] *Fraunhofer Institute for High Frequency Physics and Radar Techniques (FHR), 53343 Wachtberg, Germany*
Email: delphine.cerutti-maori@fhr.fraunhofer.de
[(2)] *European Space Agency - ESA/ESOC, 64293 Darmstadt, Germany*

ABSTRACT

Presently, there exists very little knowledge about the density and distribution of space debris of the size of a few millimeters. The reason is that ground-based systems are not sensitive enough to detect such small objects. Space-based radars have the potential through in situ measurements to validate or discard the current space debris models and to help filling this knowledge gap. This paper presents a preliminary design of a space-based radar for detecting mm-size space debris and discusses the potentials and limitations of such a concept.

Key words: Space debris, space-based radar.

1. INTRODUCTION

1.1. mm-size space debris

Space systems are generally shielded to survive a collision with space debris up to a size of 1 cm. Over that limit, a collision is usually lethal for a space system depending on the relative velocity between the two objects. Collisions with small debris within the critical size range of 1 mm to 1 cm may not be harmless to a space system as it can degrade its mission by damaging its payload and on-board instruments. Therefore, it is of high importance to know how many of these mm-size debris are orbiting around the Earth and where they are orbiting.

The debris population models MASTER (Meteroid and Space Debris Terrestrial Environment Reference) and ORDEM (Orbital Debris Engineering Model) were independently developed by ESA and NASA, respectively. They both model the flux of debris in Earth orbit under the assumption of different debris classes and source populations, and were generated using different techniques. Figure 1 shows an example of a comparison between these two debris population models (figure taken from [1]). While a good agreement can be observed between the models for debris larger than 6 mm, the models diverge from each other for debris within the critical size range. Ground-based optical and radar sensors regularly track and catalogue larger space objects with their orbit parameters. These systems also gain periodically statistical information about debris larger than 6 mm during measurement campaigns like beampark experiments [2]. The information is used to validate current space debris models, which explains the good fit between these two population models for debris larger than 6 mm[1]. Ground-based sensors are, however, not sensitive enough to detect smaller mm-size debris. This fact evidences the current need to gain information about this critical debris population through independent sensor measurements in order to validate and further develop these space debris models.

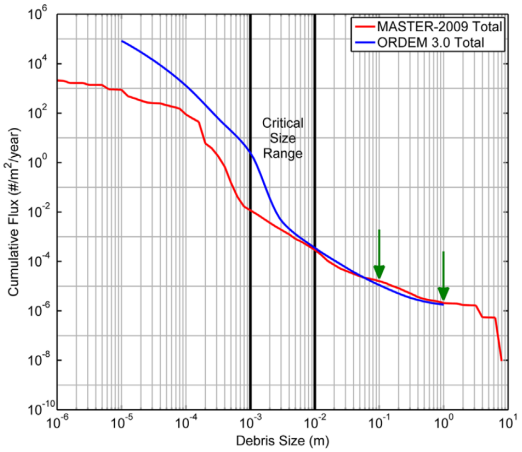

Figure 1. Debris population models for an exemplary sun synchronous orbit (from [1])

So far, these models have been checked within the critical size regime for some discrete orbits by counting and analysing the debris impacts on retrieved space systems (e. g. Shuttle transportation system) [2]. Orbital radar and optical sensors have a high potential for validating these models trough in situ measurements. The instrument can be either installed on a mini satellite or added

[1] Note that the population models can only be validated for the orbits that can be monitored by these ground-based systems due to geometrical constraints.

as an experiment to another space mission and it can be injected to the orbit of interest. [3] investigated the potentials of space-based optical systems for space debris observation. This paper examines the performance of radar systems for detecting space debris following specifications made by ESA. Radar systems have the advantage compared to optical systems to operate at any time a day independently of the sun illumination. They have, however, a larger power consumption.

1.2. ESA's specifications for a space-based radar to detect mm-size space debris

The goal of the space-based radar to be designed is to detect and count the individual objects with a diameter of 1 to 10 mm up to a range of 500 m. The maximum radar peak power is 50 W. The angular velocities of the debris of particular interest range between 0.1 deg/s and 10 deg/s with an average of 3 deg/s. The radar system mass should not exceed 10 kg.

These specifications raise several questions, which should be answered by the investigation performed in this paper. Is it possible to design such a radar? In which frequency band should the radar operate? How should the signal processing be performed? What is the expected detection performance? What is the expected detection rate according to ESA's model?

The paper is organized as follows. The impact of the radar frequency on the occurring backscattering process is investigated in Section 2. Section 3 discusses the influence of the antenna orientation on the expected radial and transversal velocities between space object and radar and selects the most suitable antenna orientation. Different radar concepts are introduced in Section 4. Issues such as range and Doppler cell migration and their impact on the radar performance are examined as well. Section 5 discusses the characteristics and potentials of each investigated radar design and selects the most promising concept. Section 6 investigates the expected detection rate. Section 7 summarizes the analysis and assesses the performance of this preliminary radar concept.

2. EXPECTED RCS OF THE SPACE DEBRIS

A space debris is modelled in this study as a metallic sphere. Depending on the ratio between radar wavelength λ and debris size, different scattering mechanisms occur, which affect the object radar cross section (RCS).

Rayleigh scattering occurs when the radar wavelength is much larger than the object. In this case, the RCS is proportional to λ^{-4}. When the object is much larger than the radar wavelength, the radar waves are reflected according to a specular reflection. In this case, the RCS solely depends on the object size. The RCS of the object oscillates strongly when radar wavelength and object have approximately the same size (Mie or resonance scattering).

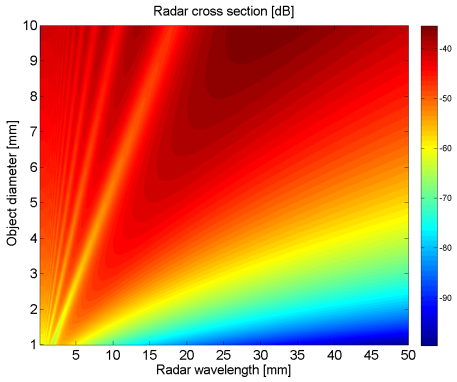

Figure 2. RCS of the space debris

Table 1. Upper and lower velocity bounds

	Radial velocity	Transversal velocity
$\mathbf{u}_{\text{LOS}}=[1\ 0\ 0]^{\dagger}$	$\lvert V_{\text{r}}^{\text{min}}\rvert = 0$ m/s $\lvert V_{\text{r}}^{\text{max}}\rvert = 15$ km/s	$V_{\text{t}}^{\text{min}} = 0$ m/s $V_{\text{t}}^{\text{max}} = 7.5$ km/s
$\mathbf{u}_{\text{LOS}}=[0\ 1\ 0]^{\dagger}$	$\lvert V_{\text{r}}^{\text{min}}\rvert = 0$ m/s $\lvert V_{\text{r}}^{\text{max}}\rvert = 1$ km/s	$V_{\text{t}}^{\text{min}} = 0$ m/s $V_{\text{t}}^{\text{max}} = 15$ km/s
$\mathbf{u}_{\text{LOS}}=[0\ 0\ 1]^{\dagger}$	$\lvert V_{\text{r}}^{\text{min}}\rvert = 0$ m/s $\lvert V_{\text{r}}^{\text{max}}\rvert = 7.5$ km/s	$V_{\text{t}}^{\text{min}} = 0$ m/s $V_{\text{t}}^{\text{max}} = 15$ km/s

These oscillations are caused by interferences between backscattered waves and creeping waves.

Because the size of the space debris of interest is in the order of a few millimeters, frequency bands below the C band (i. e. frequencies lower than 6 GHz corresponding to wavelengths larger than 5 cm) are not adapted and are discarded in this study. Radar wavelengths smaller than 1 mm (Terahertz frequency band) are not considered either caused by the resulting too small antenna beamwidth. The expected RCS [4] of the space debris of interest are presented in Figure 2 according to the radar wavelength. In this paper we assume that the RCS of the debris is deterministic (Swerling case 0) [5] and does not vary from pulse to pulse or from dwell to dwell. Therefore, the presented radar performances are to be understood as upper bound.

3. ANTENNA ORIENTATION

This section investigates the range of possible radial and transversal velocities between the satellite and a space debris for different antenna orientations.

Suppose that the satellite is moving on a circular orbit with the velocity V_{sat} =7500 m/s. In order to describe the motion between the satellite and the space object, we introduce the satellite coordinate system, whose origin is located at the centre of mass of the satellite. This coordinate system has its x-axis pointing in the direction of satellite motion, its y-axis that points towards

the Earth centre, and its z-axis that completes the right-angled coordinate system. We have therefore $\mathbf{v}_{\text{sat}} = [V_{\text{sat}}, 0, 0]^\dagger$ m/s.

Since satellite and space object are apart of a maximum distance of 500 m, we assume for the sake of simplicity[2] that the space debris also move with the velocity $V_{\text{deb}} = \|\mathbf{v}_{\text{deb}}\|_2 = V_{\text{sat}}$. The direction of motion is, however, different from the one of the satellite. To account for a potential elliptical orbit, we define their possible motion within

- x-direction: $\mathbf{v}_{\text{deb}}^\dagger \mathbf{x} \in$ [-7500,7500] m/s
- y-direction: $\mathbf{v}_{\text{deb}}^\dagger \mathbf{y} \in$ [-1000,1000] m/s
- z-direction: $\mathbf{v}_{\text{deb}}^\dagger \mathbf{z} \in$ [-7500,7500] m/s

where the vectors $\mathbf{x}$, $\mathbf{y}$, and $\mathbf{z}$, denote the unity vectors in the x-, y-, and z-directions respectively.

Projecting the relative velocity vector between the space debris and the satellite $\mathbf{v}_{\text{deb}} - \mathbf{v}_{\text{sat}}$ onto the x-, y-, and z-axis yields to the radial velocities, which would be measured by a radar, whose antenna is arranged along the x-, y-, and z-axis, respectively. The radial velocity is defined according to

$$V_{\text{r}} = (\mathbf{v}_{\text{deb}} - \mathbf{v}_{\text{sat}})^\dagger \cdot \mathbf{u}_{\text{LOS}}, \tag{1}$$

where $\mathbf{u}_{\text{LOS}}$ is the line-of-sight (LOS) vector. The corresponding transversal velocity (i. e. perpendicular to the range direction) is computed according to

$$V_{\text{t}} = \|(\mathbf{v}_{\text{deb}} - \mathbf{v}_{\text{sat}})^\dagger \cdot \left(\mathbf{I} - \mathbf{u}_{\text{LOS}}\mathbf{u}_{\text{LOS}}^\dagger\right)\|_2. \tag{2}$$

The matrix $\mathbf{I}$ denotes here the identity matrix.

The corresponding minimum and maximum velocities for different antenna orientations are given in Table 1. This table reveals that the radar antenna should be orientated along the x-axis in order to get the smallest maximum transversal velocity. This would maximize the duration over which the space debris remain within the antenna beam. The price to pay by choosing this antenna orientation is a two-time larger maximum radial velocity compared to the configurations where the antenna is orientated along the y- or the z-axis. However, this does not impair the radar performance as will be shown in Section 5.2. For the remaining of the paper, we choose therefore to align the antenna LOS with the direction of motion.

4. DESIGN OF A RADAR SYSTEM FOR IN SITU MEASUREMENTS

Several kinds of radar systems exist that either can measure the range (e. g. non coherent pulse radar), the radial velocity through the Doppler shift (e. g. continuous waveform (CW) radar) or both (e. g. coherent pulse radar, frequency modulated CW (FMCW) radar). Coherent pulse radars and FMCW radars have the ability over CW radars to detect and discriminate space debris moving with similar velocities at different ranges. This is a significant advantage, if the debris density is expected to be high. Another advantage is that information about the orbit of the detected object can be gained by exploiting the evolution of the range/Doppler parameters of the debris over time. Also, information about the object size can be derived from the range and the measured signal-to-noise ratio (SNR). However, the design of such radars is more challenging. In the following we will examine the performance of these radars and assess their suitability for the present application.

[2]Note that the proposed orbital model is extremely simplified. However, it is appropriate to investigate the choice of the antenna orientation.

Table 2. Coherent pulse radar parameters

Peak power	P_{TX}	50 W
Duty cycle	ν	1.65%
Pulse length	τ	66 ns
Range resolution	δ_{r}	10 m
Antenna diameter	D	80 cm
Aperture efficiency	η	0.7
Maximum PRF	$f_{\text{PRF}}^{\text{max}}$	290 kHz
PRF	f_{PRF}	250 kHz
Dead time	T_{sys}	1 ns
Minimum range	R_{min}	10 m
Maximum range	R_{max}	500 m
Losses	κ	-2 dB
Noise figure	N_{f}	3 dB

4.1. Coherent pulse radars

The available SNR of a debris after range compression and for one pulse is given by

$$SNR_0 = \frac{P_{\text{TX}} G_{\text{TX}} G_{\text{RX}} \lambda^2 \tau \kappa \rho}{(4\pi)^3 R^4} \frac{1}{K N_{\text{f}}} \sigma_{\text{t}}. \tag{3}$$

where P_{TX} is the peak transmit (TX) power, G_{TX} is the transmit gain, G_{RX} is the receive (RX) gain, R is the range, τ is the pulse length, and σ_{t} is the RCS of the target. The parameters κ and ρ take into account additional system and processing losses respectively. The antenna gain is related to the effective antenna surface A_{e} according to

$$G_{\text{TX}} = G_{\text{RX}} = \frac{4\pi A_{\text{e}}}{\lambda^2} = \frac{4\pi A \eta}{\lambda^2}. \tag{4}$$

η denotes the aperture efficiency and A denotes its physical area. N_{f} is the noise figure. The constant K is the

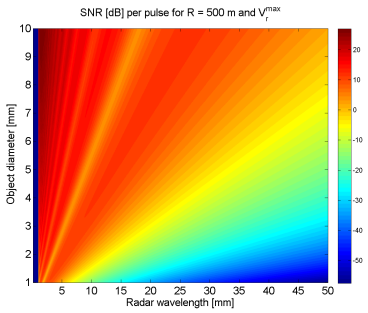

(a) SNR per pulse, R = 500 m and $V_{\mathrm{r}}^{\max}$ (worst case)

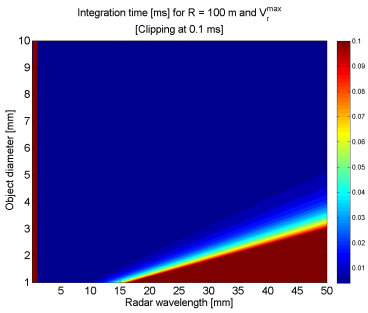

(b) Integration time, R = 100 m and $V_{\mathrm{r}}^{\max}$ (worst case)

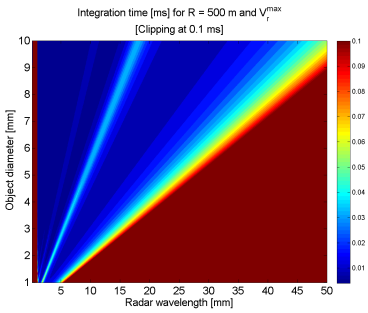

(c) Integration time, R = 500 m and $V_{\mathrm{r}}^{\max}$ (worst case)

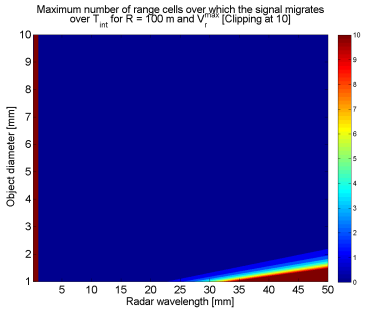

(d) Range migration over T_{int}, R = 100 m and $V_{\mathrm{r}}^{\max}$ (worst case)

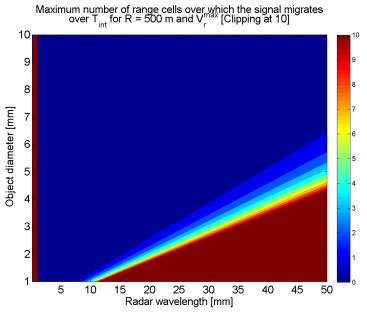

(e) Range migration over T_{int}, R = 500 m and $V_{\mathrm{r}}^{\max}$ (worst case)

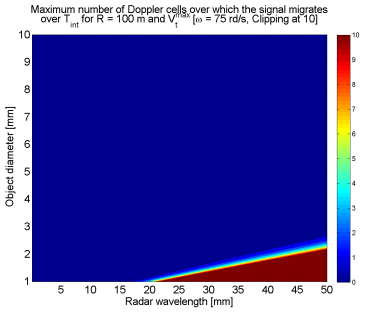

(f) Doppler migration over T_{int}, R = 100 m and $V_{\mathrm{t}}^{\max}$ (worst case)

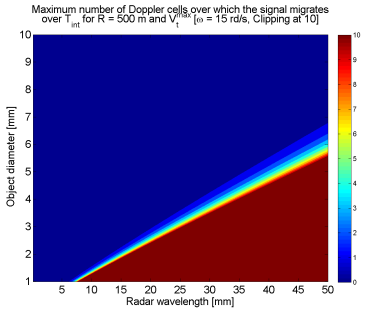

(g) Doppler migration over T_{int}, R = 500 m and $V_{\mathrm{t}}^{\max}$ (worst case)

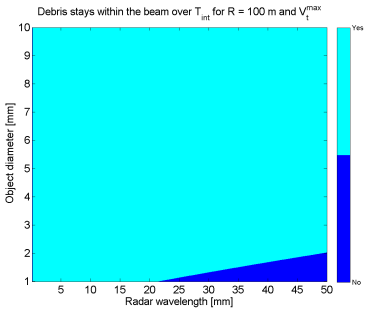

(h) Integration time vs. illumination time, R = 100 m and $V_{\mathrm{t}}^{\max}$ (worst case)

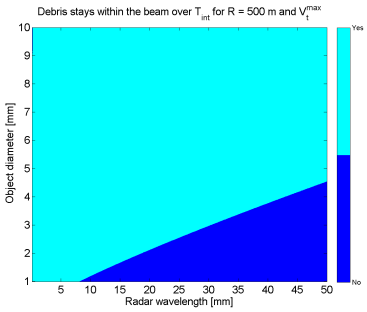

(i) Integration time vs. illumination time, R = 500 m and $V_{\mathrm{t}}^{\max}$ (worst case)

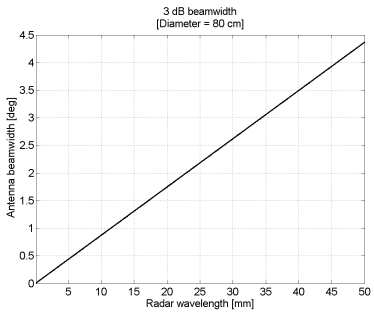

(j) Antenna beamwidth

Figure 3. Coherent pulse radar

product of the Boltzmann's constant by the system equivalent noise temperature (297 K); $K = 4e^{-21}$ Ws. Uncorrelated white Gaussian noise in each quadrature component is assumed. Therefore the amplitude probability density function (PDF) of the noise signal is Rayleigh-distributed and the amplitude PDF of the target-plus-

noise signal is Rice-distributed.

In order to reduce the impact of range migration, we choose here an unmodulated rectangular pulse as waveform, whose bandwidth B is inversely proportional to the pulse length τ. Rectangular pulses are non-Doppler tolerant waveforms. A matched filter bank should be used in order to maximize the SNR of the signal after range compression. However, in order to simplify the processing architecture, we waive using a matched filter bank and solely use the non-Doppler shifted signal to compress the receive signal. The resulting processing loss can be modelled as a first approximation by the linear relationship

$$\rho = 1 - \frac{|f_{\text{dop}} - \bar{f}_{\text{dop}}|}{B} \qquad \text{for} \quad |f_{\text{dop}}| \leq B, \tag{5}$$

where the Doppler frequency is defined by

$$f_{\text{dop}} = -\frac{2}{\lambda} V_{\text{r}} \tag{6}$$

and $\bar{f}_{\text{dop}}$ is the expected mean Doppler frequency.

For a parabolic antenna, the antenna beamwidth is defined by

$$\Theta_{\text{BW}} = 1.22 \frac{\lambda}{D}, \tag{7}$$

where D is the antenna diameter.

Let N_{req} be the number of pulses that is required to reach the SNR threshold after coherent integration. The integration is performed here by a simple FFT over slow time[3]. The SNR over that CPI is given by

$$SNR = N_{\text{req}} SNR_0 = N_{\text{req}} \frac{\nu P_{\text{TX}} A^2 \eta^2 \kappa \rho}{4\pi R^4 K f_{\text{PRF}} N_{\text{f}} \lambda^2} \sigma_{\text{t}}, \tag{8}$$

where f_{PRF} is the pulse repetition frequency and ν is the duty cycle

$$\nu = \tau f_{\text{PRF}}. \tag{9}$$

Note that in order to achieve the full coherent processing gain, the signal should not migrate between different range/Doppler cells. Range migration occurs if the variation of the range of the target over T_{int} is larger than the range resolution. Similarly, if the radial velocity rate of a debris induces a Doppler variation over T_{int} that is higher than the Doppler resolution, then the signal migrates over several Doppler resolution cells.

The data processing architecture based on a simple three-step process is sketched in Figure 4(a). Target detection is performed for each range/Doppler cell independently by comparing the output of each range/Doppler cell with the detection threshold. A simple tracking filter has been added to avoid multi-detection of the same target. The filter checks each detection by analysing if the detection is a potential sidelobe detection of a neighbouring cell or if the detection is connected to another detection at a different CPI.

[3]We assume here that the range rate is (almost) constant over a coherent processing interval (CPI). If it is not the case, it is possible to take into account the variation of the radial velocity over time by using a matched filter bank. However, such a processing is much more complicated and time-consuming and it is discarded here.

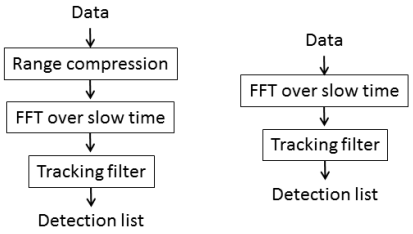

(a) Pulse radar (b) CW radar

Figure 4. Signal processing scheme

Table 3. CW radar parameters

Peak power	P_{TX}	50 W
Antenna diameter	D	28 cm
Antenna efficiency	η	0.7
Sampling frequency	f_s	4 MHz
Losses	κ	-2 dB
Noise figure	N_{f}	3 dB

Figure 3 investigates the detection performance of the pulse radar specified in Table 2. The expected SNR per pulse at far range is shown in Figure 3(a). The SNR was computed for objects moving relatively to the radar with the radial velocity $V_{\text{r}}^{\text{max}}$ (the loss through pulse compression is the highest). One notices that radar systems operating with extremely small wavelengths are almost able to detect directly the space debris of interest. However, the antenna beamwidth of such radars is extremely limited (Figure 3(j)). Figures 3(b) and 3(c) show the integration time needed to reach the SNR threshold for different ranges. To assess the required integration time we selected a SNR threshold of 13 dB since a very good detection performance (P_{D}) of almost 0.9 can be achieved at a low probability of false alarm (P_{FA}) of 10^{-6}. Figures 3(h) and 3(i) investigate for different ranges if the space debris remain sufficiently long in the antenna beam so that the required integration time can be reached. Figures 3(d) and 3(e) indicate the number of range cells over which the signal of the space object migrate during T_{int} for $V_{\text{r}}^{\text{max}}$. Finally, Figures 3(f) and 3(g) investigate the number of Doppler cells over which the debris signal is smeared after integration over T_{int}. The Doppler migration is shown for relative motions with the highest transversal component $V_{\text{t}}^{\text{max}}$ (i. e. largest Doppler frequency variation over time). Figure 3 reveals that the radar performance is superior for lower wavelengths.

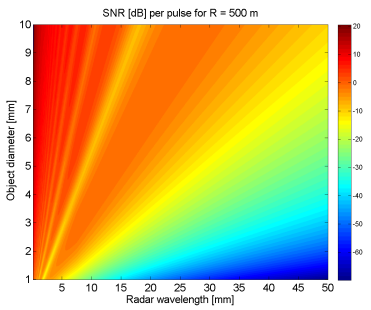

(a) SNR per pulse, R = 500 m

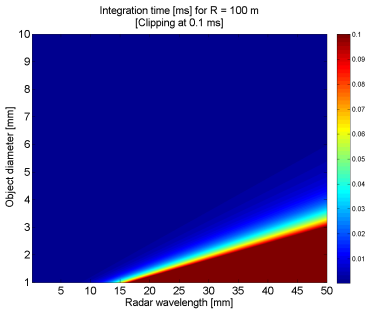

(b) Integration time, R = 100 m

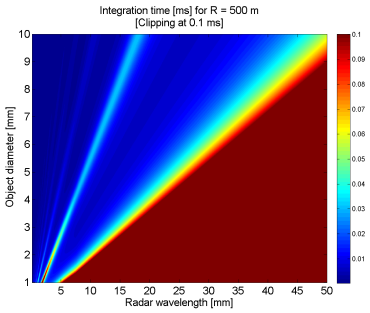

(c) Integration time, R = 500 m

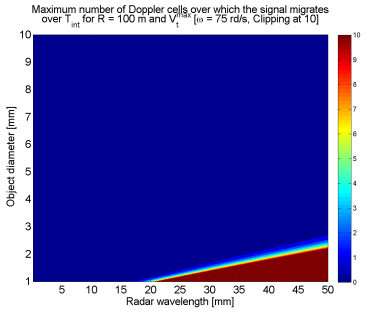

(d) Doppler migration over T_{int}, R = 100 m and $V_{\mathrm{t}}^{\mathrm{max}}$ (worst case)

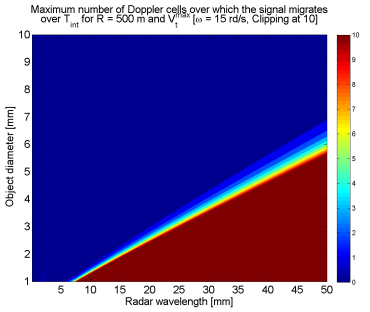

(e) Doppler migration over T_{int}, R = 500 m and $V_{\mathrm{t}}^{\mathrm{max}}$ (worst case)

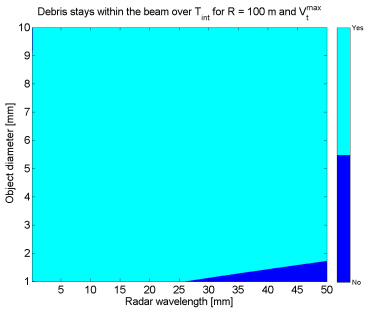

(f) Integration time vs. illumination time, R = 100 m and $V_{\mathrm{t}}^{\mathrm{max}}$ (worst case)

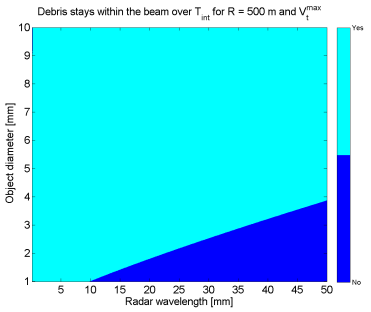

(g) Integration time vs. illumination time, R = 500 m and $V_{\mathrm{t}}^{\mathrm{max}}$ (worst case)

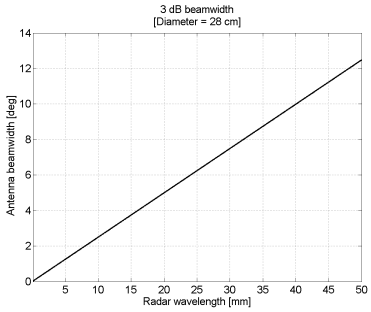

(h) Antenna beamwidth

Figure 5. CW radar

4.2. CW radars

CW radar systems emit a single frequency signal. The available SNR of a target after integration over T_{int} can be modelled according to

$$SNR = \frac{P_{\mathrm{TX}} A^2 \eta^2 \kappa \sigma_{\mathrm{t}}}{4\pi R^4 \lambda^2} \frac{1}{K N_{\mathrm{f}}} T_{\mathrm{int}}, \tag{10}$$

where T_{int} denotes the required integration time to achieve the SNR threshold. The bandwidth of the analogous filter B_{dop} has to be chosen so that all the Doppler frequencies of interest can be received by the radar, i. e.

$$B_{\mathrm{dop}} = \frac{2}{\lambda}(V_{\mathrm{r}}^{\mathrm{max}} - V_{\mathrm{r}}^{\mathrm{min}}). \tag{11}$$

The signal processing for CW radars reduces here to a simple FFT for coherent integration after A/D sampling. The corresponding signal processing scheme is presented in Figure 4(b).

Results of the system described in Table 3 are shown in Figure 5. The same SNR threshold (13 dB) and the same consistency criteria (except for the range migration) as in Section 4.1 were used. Again, one can observe that the radar performance is superior for lower wavelengths.

4.3. FMCW radars

FCMW radars could be an alternative to pulse radars. The major advantage is the larger mean power as FCMW

radars transmit continuously. However, the receive signal has to be analyzed carefully[4]. Terms that are usually neglected for lower radial velocities may not be negligible for radial velocities up to 15 km/s. Without proper compensation, they may introduce some range/Doppler defocusing and decrease the SNR. Therefore, FMCW radars are not investigated in more details in this paper.

5. DISCUSSION

5.1. Pulse radar vs. CW radar

Analyzing Figures 3 and 5 reveals that the space-based radar should operate in the Ka band (wavelength range from 7.5 mm up to 11 mm). Lower frequency bands would be less suitable for detecting the smallest debris of interest. Higher frequency bands have the disadvantage of a narrower antenna beamwidth, which reduces the monitored field of view (FOV). One can see that both systems fulfill ESA requirements and have similar detection performance. In both cases, the factor limiting the integration gain is the Doppler cell migration (Figures 3(g) and 5(e)). One notices that the required coherent gain at far range cannot be completely achieved through simple FFT for the small debris around 1 mm diameter moving relatively to the radar with high transversal velocities at far range. However, a much more complicated processing that would use a matched filter bank of chirp filters with the aim to increase the SNR would not gain much as the debris do not stay long enough within the antenna beam (Figures 3(i) and 5(g)).

Due to their characteristics, CW radars are more adapted for the present application of validating space debris models (low density population). They offer the advantage of a reduced size and weight with a lower hardware complexity compared to pulse radars. For the same detection capability, they can monitor a much wider FOV (see system specifications in Tables 2 and 3). However, CW radars do not measure the range of the debris, a parameter which can be used to derive additional information about the detected object (i. e. size). Higher TX/RX isolation is also needed compared to pulse radars since they transmit and receive at the same time.

Nevertheless, based on the requirements for the considered application, we select here a CW radar. The refined system parameters of the radar are given in Table 4.

Table 4. Parameters of the selected CW radar

Peak power	P_{TX}	50 W
Antenna diameter	D	28 cm
Antenna efficiency	η	0.7
Losses	κ	-2 dB
Noise figure	N_{f}	3 dB
Wavelength	λ	8 mm
Antenna beamwidth	Θ_{BW}	2°
Sampling frequency	f_s	4 MHz
Integration time		0.4 ms
PFA	P_{FA}	10^{-13}
SNR threshold		16 dB
False alarm occurrence		$\sim$ 0.035 per day

5.2. Detection performance of the selected CW radar

Figure 6 shows the detection performance of the selected CW radar system. The detection capability is plotted for the most favorable motion (upper bound, Figures 6(a) and 6(b)) and least favorable motion (lower bound, Figures 6(c) and 6(d)) between debris and radar. While the debris larger than 1.3 mm can be detected at a range of 500 m when the relative motion is only radial, only debris larger than 1.7 mm will be detected at the same range for relative motions with the highest transversal velocity. By increasing the antenna size, all debris within the considered size regime could be detected independently of their motion, however, at the cost of a reduced FOV. Extending the integration time has a two-sided effect on the debris detection. While debris with pure radial velocity component could be detected at higher ranges, debris with large transversal velocity component could only be detected at nearer ranges.

Note that orienting the antenna to different directions affects the overall performance of the radar. This effect can be observed in Figure 7. In both cases, ESA's requirements would not be fulfilled. This is due to the larger occurring transversal velocities between debris and radar which cause higher Doppler frequency variations over time.

CW radars detect all debris crossing the FOV that reflect enough power back. Larger objects at larger range will be detected as well as revealed by Figure 8. The simple RCS model of section 2 was used here. An important aspect has to be pointed out here. Since the range of the detected debris is not known, it is not possible to estimate the object size from the range and the SNR by using an appropriate RCS model. Therefore, CW radars cannot make a discrimination between debris below 1 cm and debris larger than 1 cm. The presence of larger detected objects has to be taken into account in order to estimate the true detection rate of the small size debris population.

Pulse radars and FMCW radars, on the other hand, could differentiate between objects of different sizes[5]. However, the sampling frequency of these radars has to be strongly decreased, so that the signal coming from the farthest to be detected object is still range unambigu-

[4]Note that within a single pulse, the radial velocity component induces an additional Doppler shift, which is superimposed on the beat frequency. This effect causes a wrong range measurement.

[5]The RCS of an object depends on a wide number of parameters (such as wavelength, used polarization, geometry between radar and object, object material and shape, ...). It can vary a lot over time and is complex to model for complex objects.

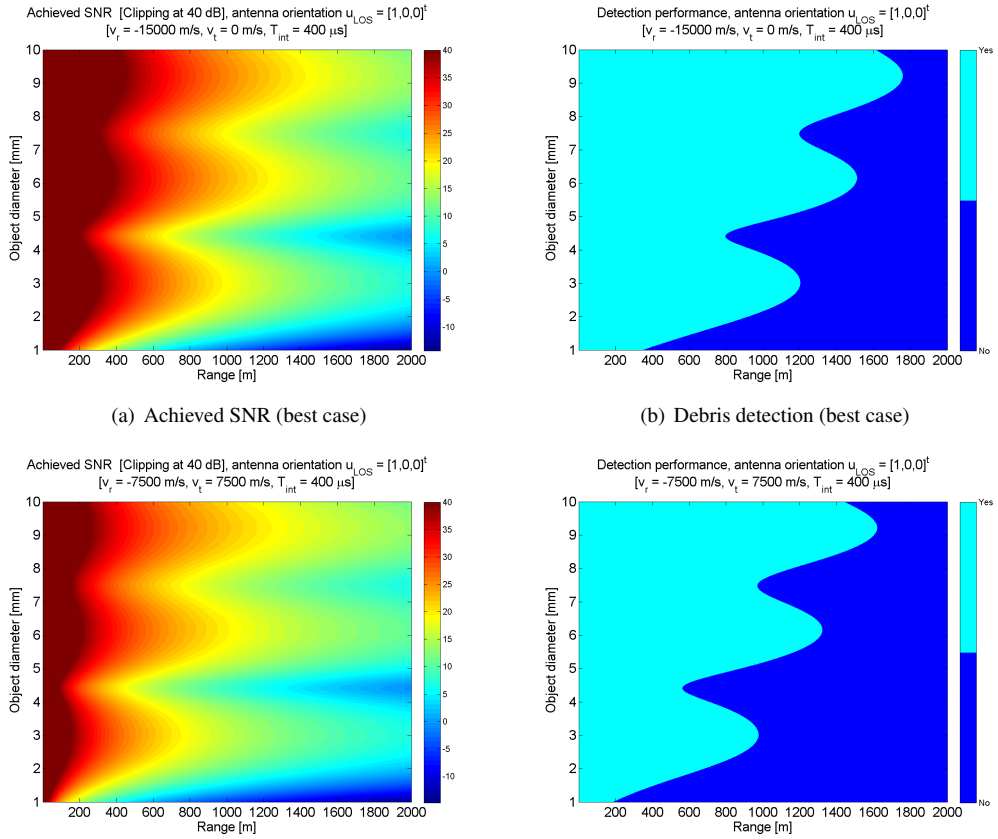

(a) Achieved SNR (best case)

(b) Debris detection (best case)

(c) Achieved SNR (worst case)

(d) Debris detection (worst case)

Figure 6. Radar detection performance (debris of interest), antenna oriented along the x-axis (direction of motion)

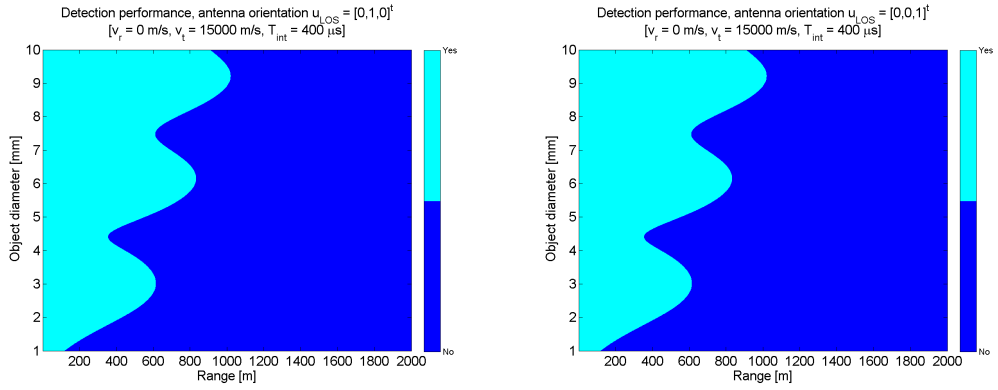

(a) Antenna oriented along the y-axis

(b) Antenna oriented along the z-axis

Figure 7. Radar detection performance (debris of interest). In both cases, the plotted performance corresponds to the worst case scenario (maximum transversal velocity).

ous. Otherwise, the measured range information could not be used for size classification. Alternatively, the dwell time could be evaluated to retrieve the true range from the measured unambiguous range. Reducing the sampling frequency would degrade the radar performance a lot, which confirms our choice of selecting a CW radar system.

As described in [2, 1], the expected debris density is small. Therefore a very low P_{FA} has to be chosen here in order not to alter the measured detection rate of the small size debris population. Figure 9 investigates the influence

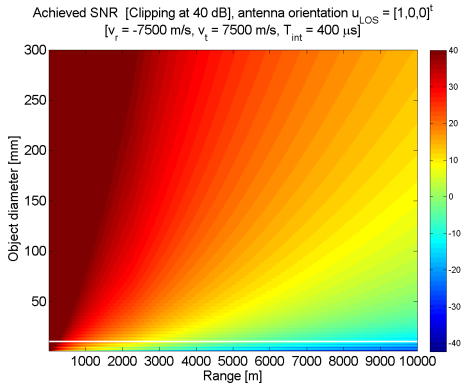

(a) Achieved SNR (worst case)

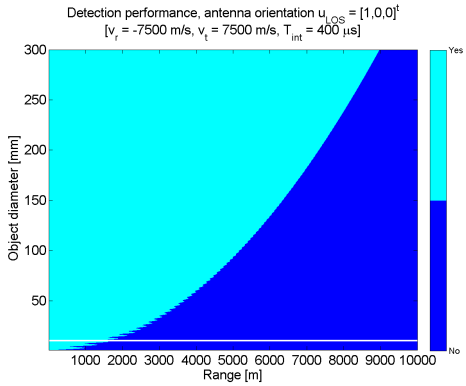

(b) Debris detection (worst case)

Figure 8. Radar detection performance (all debris), antenna oriented along the x-axis (direction of motion). The white line indicates the region of the debris of interest.

Table 5. Simulation parameters for PROOF

Number of Monte Carlo simulations	1
Duration	12 h
Epoch	May 1, 2009

of the false alarm probability on the expected number of false alarms. The lower the P_{FA}, the lower the number of false alarms and the higher the detection threshold. We choose a required SNR of 16 dB in order to get about one false alarm every month.

6. INVESTIGATION OF THE DEBRIS DETECTION RATE

This section investigates the detection rate of the CW radar system defined in Section 5.

The geometric filter of the software PROOF (Program for Radar and Optical Observation Forecasting) [6] was used to select the debris crossing the FOV of the radar. The main objective of the PROOF software is to simulate the performance of radar and optical instruments for space

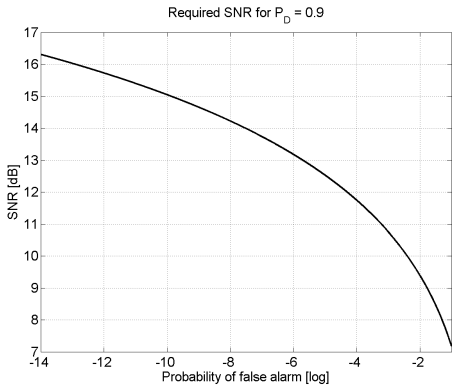

(a) Required SNR

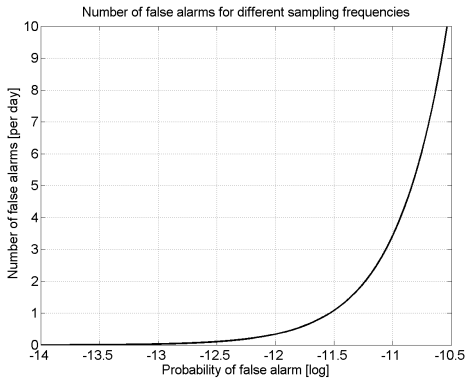

(b) Number of false alarms per day

Figure 9. Influence of P_{FA}

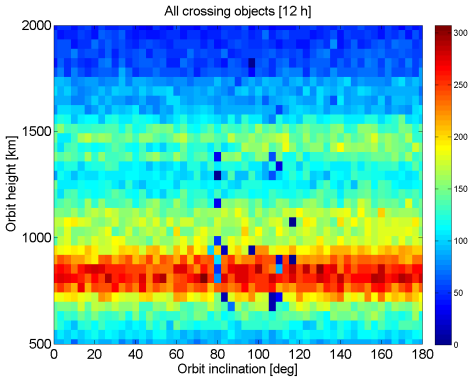

Figure 10. Number of crossing objects within the FOV cone up to a range of 50 km

debris detection and thus to validate space debris models by comparing the output of PROOF with real measurements acquired by the modeled sensors. The sensor can be either ground-based or space-based. Since the implemented radar performance scheme in PROOF (incoherent integration) is different from the one used for our space-based radar (coherent integration), a radar performance simulator was developed separately, which mod-

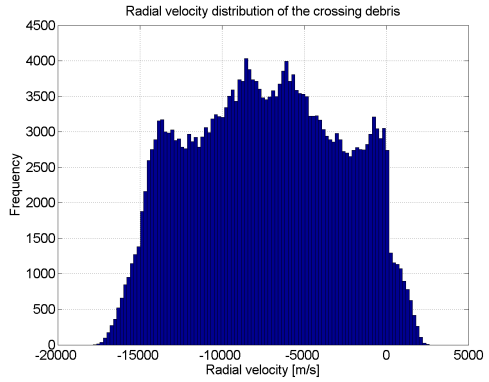

(a) Radial velocity

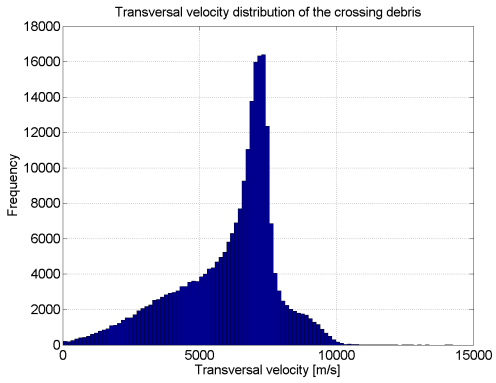

(b) Transversal velocity

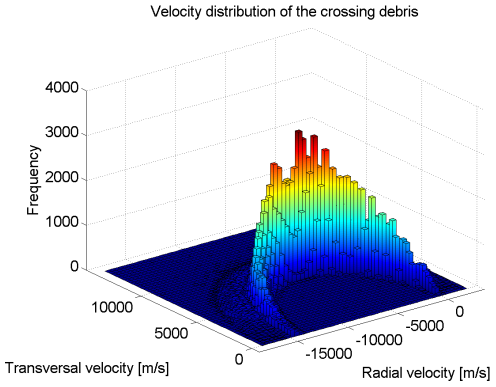

(c) Radial versus transversal velocity

Figure 11. Velocity distribution

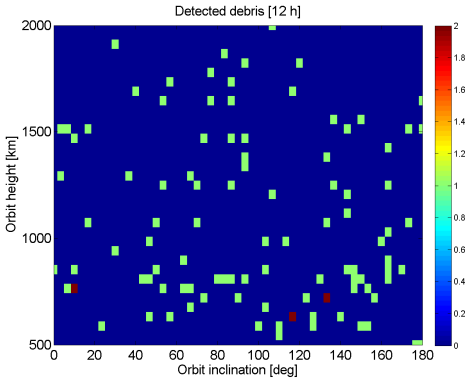

Figure 12. Number of detected crossing objects

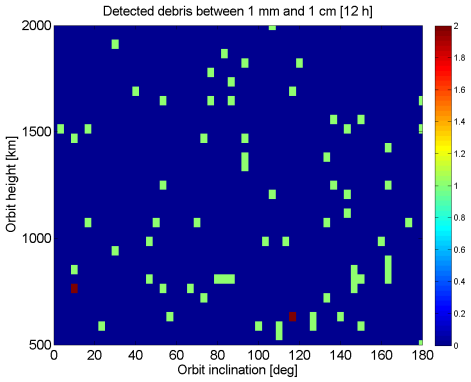

Figure 13. Number of detected crossing objects with diameter between 1 mm and 1 cm

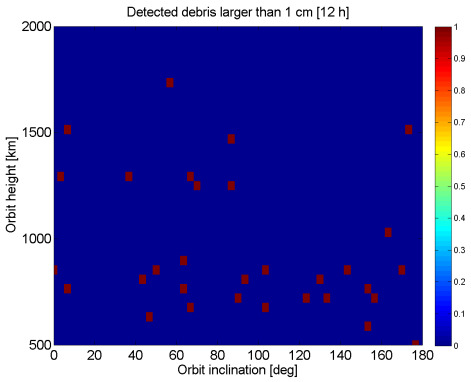

Figure 14. Number of detected crossing objects with diameter larger than 1 cm

eled the radar sensitivity and performed the detection decision from the parameters of the crossing objects.

The crossing rates for the considered radar is shown in Figure 10 for orbit heights ranging from 500 km up to 2000 km and orbit inclinations within 0° and 180° for the parameters listed in Table 5. Expectedly, the highest debris density is found around the orbit height of 800 km. Figure 11 presents the velocity distribution of the crossing objects. Caused by the orbit eccentricity of the debris, one observes both a broadening of the radial velocity interval (Figure 11(a)) and of the transversal velocity interval (Figure 11(b)) compared to Table 1. From these velocity distributions, the bandwidth B_{dop} of the final radar and the optimum integration time T_{int} have to be computed in order not to miss any debris.

The corresponding detection rates are presented in Fig-

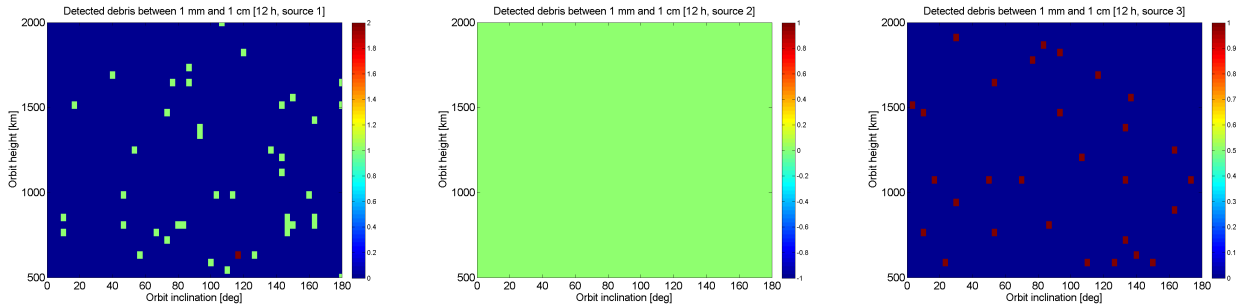

(a) Fragments (b) NaK droplets (c) SRM slag

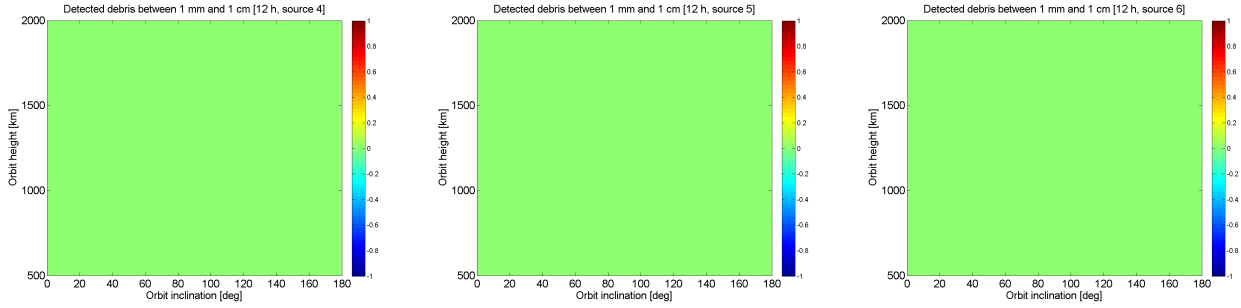

(d) TLE objects (e) Westford needles (f) Multi-layer insulation

Figure 15. Number of detected crossing objects with diameter between 1 mm and 1 cm

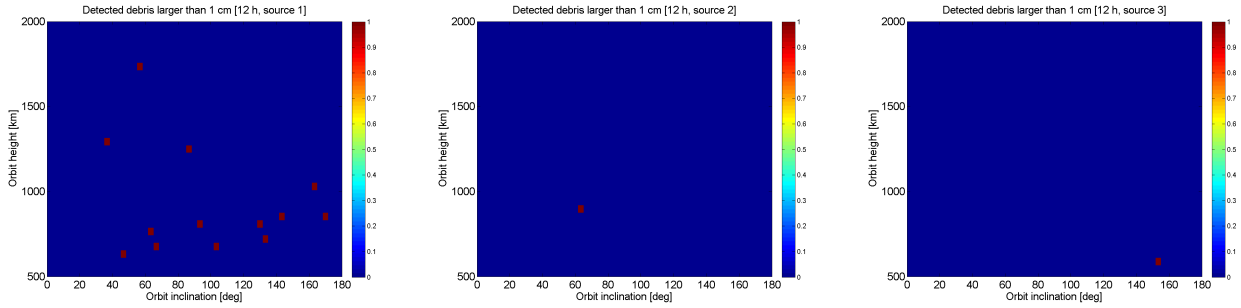

(a) Fragments (b) NaK droplets (c) SRM slag

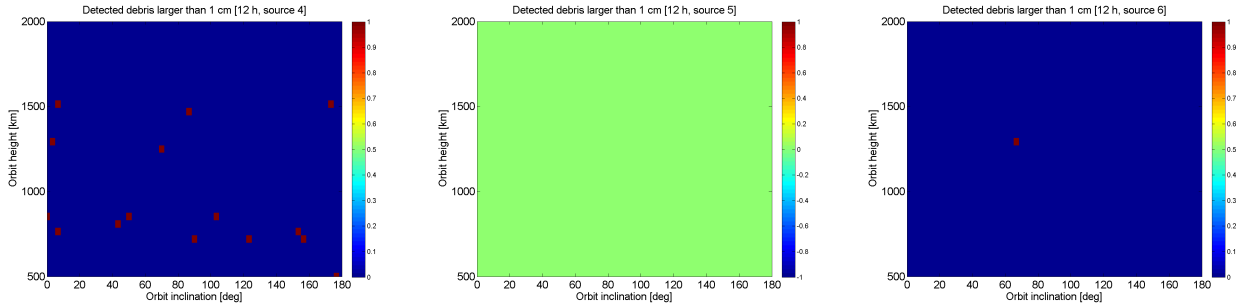

(d) TLE objects (e) Westford needles (f) Multi-layer insulation

Figure 16. Number of detected crossing objects with diameter larger than 1 cm

ures 12 to 14. Figures 15 and 16 show the origin of the detected objects. As expected, fragmentation particles and solid rocket motor (SRM) slag are the larger sources of debris in the critical size range. All these figures have

to be understood on a statistical basis. They are the result of one realization over a short time period. In order to obtain a more relevant statistical significance, several realizations over a longer duration should be averaged. Such a simulation would be, however, extremely time-consuming. Therefore, as a rule of thumb, one can say that about less than 1 up to 5-6 objects can be expected to be detected on average within 24 h depending on the chosen orbit parameters of the space-based radar. As discussed previously, the radar will output the debris detection rate of Figure 12. To have access to the statistics of the critical debris (Figure 13), the expected detection rate of the objects with diameter larger than 1 cm (Figure 14) has to be subtracted.

7. CONCLUSION

Space debris below 1 cm have the potential to damage satellites and degrade their performance. Current space debris models of ESA and NASA show a discrepancy in the expected density of these critical objects. In order to further develop and validate these debris models, the modeled debris population should be checked against real measurements. Critical size debris are usually too small to be detected by ground-based optical and radar instruments, which are limited by their sensor sensitivity. Orbital radar and optical sensors could therefore play a major role in validating these debris population models through in situ measurements.

This paper investigated the potentials and limitations of two kinds of radar systems, which both fulfil the specifications set by ESA on the radar system to be designed. The first analyzed system is a pulse radar that also measures the range of the detected objects, while the second analyzed system is a CW radar. CW radars can illuminate a larger FOV compared to pulse radars of same sensitivity, as these radars are continuously transmitting. They are definitely more adapted to this application, which is to count the number of detected objects in a low-density environment. The overall expected performance of the selected CW radar system was also assessed. It was shown that larger objects will be detected as well, which impacts the statistics. Since CW radars do not give any information about the range of the detected objects, it is not possible to derive any information about the size of the objects from the measured SNR (e. g. through a simple RCS model). Therefore CW radars can only give statistical information on the overall density of space objects. This statistics has to be externally corrected by the statistics of debris larger than 1 cm (available from the space debris models) in order to have access to the statistics of critical size debris.

The antenna orientation of the radar was selected to optimize the radar performance. In order to finalize the choice of the antenna orientation, the debris detection rates achieved with antenna orientations that maximize the number of crossing objects should be investigated and compared to the results presented in this paper.

ACKNOWLEDGMENT

This work was financed by ESA-ESOC (Contract No. 4000109778/13/D/SR).

The authors would like to thank particularly Carsten Wiedemann and his colleagues (Institute of Space Systems, Technische Universität Braunschweig) for their great support for the use of the software PROOF.

REFERENCES

1. P.H. Krisko, S. Flegel, M.J. Matney, D.R. Jarkey, and V. Braun: *ORDEM 3.0 and MASTER-2009 modeled debris population comparison*, Acta Astronautica, vol. 113, August-September 2015, pp. 204-211.
2. H. Klinkrad: *Space debris, Models and Risk Analysis*, Springer, 2006.
3. H. Krag, M. Kahl, J. Bendisch, H. Klinkrad, and T. Schildknecht: *Space based optical observation of small debris objects*, September 2001, https://www.researchgate.net/publication/234500020.
4. D.E. Kerr: *Propagation of short radio waves*, The Institution of Engineering and Technology, 1986.
5. M. Skolnik: *Introduction to Radar Systems*, McGraw-Hill Science/Engineering/Math, Third edition, 2002.
6. J. Gelhaus, S. Flegel, and C. Wiedemann:*Program for Radar and Optical Observation Forecasting, final report*, May 2011, ESA contract 21705/08/D/HK.